Molecular conductance calculations of single-molecule junctions using projection-based density functional embedding

Dávid P. Jelenfi,[1,2] Attila Tajti,[2] and Péter G. Szalay[2]
[1)] *Hevesy György PhD School of Chemistry, ELTE Eötvös Loránd University, Pázmány Péter sétány 1/A, Budapest H-1117, Hungary*
[2)] *Laboratory of Theoretical Chemistry, Institute of Chemistry, ELTE Eötvös Loránd University, Pázmány Péter sétány 1/A, Budapest H-1117, Hungary*

(*Electronic mail: attila.tajti@ttk.elte.hu)

(Dated: 11 December 2024)

Single-Molecule Junctions (SMJs) are key platforms for the exploration of electron transport at the molecular scale. In this work, we present a method that employs different exchange-correlation density functionals for the molecule and the lead domains in an SMJ, allowing us to choose the optimal one for each part. This is accomplished using a formally exact projection-based DFT-in-DFT embedding technique combined with the non-equilibrium Green's function (NEGF) method to predict the zero-bias conductance. The effectiveness of the approach is illustrated through transport calculations on SMJs with benzene-1,4-diamine (BDA) and its tetramethylated and tetrafluorinated variants, using the CAM-B3LYP range-separated hybrid functional for the embedded molecule and the PBE functional for the electrodes. The findings indicate a substantial improvement in the accuracy of the predicted zero-bias conductance compared to traditional modeling using the PBE functional across the entire system. The causes for the noted improvement are demonstrated through the examination of alterations in the energy levels of the embedded molecule, along with variations in the electrode-molecule interactions.

I. INTRODUCTION

The study of molecular electron transport is of significant scientific interest across various disciplines, including material science and biochemistry. Single-Molecule Junctions (SMJs), which are built from a single molecule connected to two or more metallic nanoscale leads, represent an important platform for studying charge transport at the molecular level. The primary focus of the measurements carried out for these systems is the zero-bias conductance, which is mainly determined by the alignment of the *ionization potential* (IP) and the *electron affinity* (EA) of the molecule relative to the Fermi level of the metal leads.[?,?]

The transport properties of the SMJs can be calculated using quantum transport theory, with the electronic structure usually described by mean-field models. Based on Koopmans' theorem, the IPs and EAs can be predicted as the opposites of the energies of the corresponding occupied and unoccupied molecular orbitals, respectively. This approach is particularly effective for the first IP within the Hartree-Fock approximation and is often extended to predict all IP and EA values using the corresponding orbital energies. It is widely accepted and commonly applied to all mean-field models for electron transport calculations.[?] In most cases, density-functional theory (DFT) is used to calculate these molecular orbital energies, due to its efficiency and favorable computational cost.[?,?] However, the most widely applied Perdew-Burke-Ernzerhof parametrization[?] of the GGA functional, called simply the PBE functional or just PBE hereafter, which is known to describe the electronic structure of metallic systems well, is known to overestimate the energy of the highest molecular orbital (HOMO) and underestimate that of the lowest unoccupied MO (LUMO) in molecules, which results in an overestimation of the zero-bias conductance.[?] The main reason for this discrepancy is commonly attributed to the self-interaction error and the poor description of the interaction effects in the metal-molecule interface.[?]

A more reliable electronic structure methodology should thus provide reasonable IPs and EAs for the investigated molecule, while also being appropriate for the metallic parts in the system. Several techniques were introduced to address this issue. In the DFT+Σ method,[?,?,?] different constant shifts are applied to the occupied and unoccupied energy levels. The correction involves two components: one adjusts the occupied and unoccupied energy levels on the basis of the first IP and EA of the gas-phase molecule, while the other incorporates the effect of the metal surface, typically using a classical electrostatic model.

Alternatively, many-body theory can also be employed, instead of the single-particle picture, to improve the accuracy of the energy levels. The GW method[?,?] is currently regarded as the state-of-the-art technique in this family, which applies many-body perturbation theory on top of ordinary DFT. It was found to perform effectively for both molecules[?,?] and metals,[?] while also providing a good description for metal-molecule interfaces.[?,?] Although it has been demonstrated to predict zero-bias conductance with a good agreement with experimental values,[?,?] it is significantly more computationally demanding which limits its applicability.

An alternative approach to improving the accuracy of energy levels of the molecule without the high computational cost of many-body methods is the use of more sophisticated DFT functionals, such as hybrid or range-separated hybrid (RSH) variants. These functionals have been shown to provide significantly better molecular orbital energies for gas-phase molecules.[?,?] Despite their advantages however, hybrid functionals often struggle to accurately describe the electronic structure of metals, as they are generally parameterized for gas-phase molecules or semiconducting and insulating materials.[?,?] This discrepancy can be partially mitigated

by first-principle guided tuning of the parameters of RSH functionals in the transport calculations for each investigated system separately. With these optimized parameters, the calculated conductance is found in close alignment with the measured experimental data.[? ? ?]

In this study, we propose a framework for using distinct functionals for the molecule and the leads in the SMJ, selecting the most appropriate one for each component. This approach avoids the need for fine-tuning the employed functional, thereby reducing the computational cost and increasing the transferability and theoretical appealingness of the model. We realize this by employing a quantum embedding method to evaluate the electronic structure of the SMJ. We investigate the benzene-1,4-diamine (BDA) molecule, as well as its 2,3,5,6-tetramethyl-substituated and 2,3,5,6-tetrafluoro-substituated variants (called Me_4-BDA and F_4-BDA hereafter, respectively). BDA is widely considered as a textbook example in electron transport studies due to its extensively documented properties, which have been thoroughly investigated in both experimental[? ? ?] and theoretical[? ? ?] contexts. The BDA molecule's popularity in these studies is primarily due to its favorable characteristics, particularly its classification as a good conductor, with a measured zero-bias conductance of $(6.4\pm0.2)\cdot10^{-3}$ G_0,[?] which is well-defined and not very sensitive to the precise configuration of the SMJ.[?] Me_4-BDA and F_4-BDA have also been investigated in several electron transport studies,[? ?] their measured conductances being larger and smaller to that of BDA, respectively.[?]

In Section **??** a theoretical overview of the used methodology is presented. In Section **??** computed results are reported for the isolated molecules, identifying a DFT functional suitable for these systems. Section **??** discusses results on the transport properties of the investigated molecules obtained with the embedding model, in comparison to those from ordinary PBE calculations. The paper finishes with conclusional thoughts and outlook in Section **??**.

II. METHODOLOGY

A. Transport calculations

In quantum transport theory, the investigated SMJ is divided into two leads and a transport region, the latter referred to as *extended molecule*, as shown in Figure **??**. The leads are modeled as periodic semi-infinite systems to account for the bulk conductor's influence on the extended molecule. The extended molecule (EM) consists of the molecule under study and metallic contact regions, referred to as *electrodes* throughout this paper to distinguish them from the bulk leads.

The state-of-the-art method to determine the electron transport through SMJs is the non-equilibrium Green's function (NEGF) theory.[? ?] The key quantity in these calculations is the so-called *transmission function*, T, which describes the probability of an electron being transported through the extended molecule. Within the NEGF formalism, the transmission function can be determined from the *Green's function* of

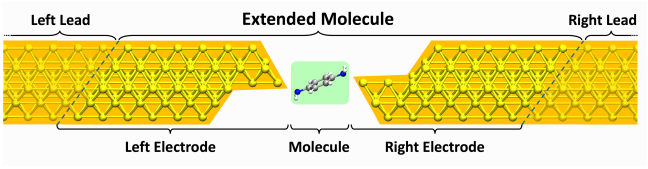

FIG. 1. Schematic representation of the division of the single-molecule junction into the extended molecule, and the leads for transport computations. The detailed structure of the extended molecule with a BDA molecule used in the calculations, is also shown.

the extended molecule, based on the Meir-Wingreen formula[?]

$$T(E,V) = \mathrm{Tr}\left[\mathbf{G}^r(E,V)\mathbf{\Gamma}_L(E,V)\mathbf{G}^a(E,V)\mathbf{\Gamma}_R(E,V)\right], \quad (1)$$

where $\mathbf{G}^{r/a}$ represent the matrix Green's functions for the extended molecule and $\mathbf{\Gamma}_L$ and $\mathbf{\Gamma}_R$ denote the left and right *coupling matrices*, respectively. In the present case, $\mathbf{G}^a = (\mathbf{G}^r)^\dagger$. The transmission function depends on the energy E of the transported electron and the bias voltage V, determined by the difference between the chemical potentials μ_L and μ_R of the left and right leads, respectively, as $V = (\mu_L - \mu_R)/e$.

The matrix Green's function of the EM that describes its electronic structure, is defined as

$$\mathbf{G}^r(E,V) = \left((E+\eta i)\mathbf{S}_{EM} - \mathbf{H}_{EM} - \mathbf{\Sigma}_L(E,V) - \mathbf{\Sigma}_R(E,V)\right)^{-1}, \quad (2)$$

where $\mathbf{H}_{EM}$ is the Hamiltonian matrix of the extended molecule and $\mathbf{S}_{EM}$ is the overlap matrix of the atomic orbitals (AOs) in the EM, while $\mathbf{\Sigma}_L^r$ and $\mathbf{\Sigma}_R^r$ are the retarded *self-energies* of the left and right leads, respectively. The term ηi, with η being an infinitesimally small number, is introduced to prevent singularities in the matrix of the Green's function at the eigenvalues of the system. The self-energies characterize the interaction between the leads and the extended molecule. The coupling matrices are derived from the self-energies as

$$\mathbf{\Gamma}_{L/R}(E,V) = -2\,\mathrm{Im}\left[\mathbf{\Sigma}_{L/R}(E,V)\right]. \quad (3)$$

The self-energies are calculated from the so-called surface Green's function of the leads via a commonly used recursion algorithm.[?] For a detailed description of the NEGF theory, the reader is referred to the excellent article of Verzijl and Thijssen,[?] as well as to Refs. **?** and **?** .

The zero-bias conductance can be determined based on the Landauer formalism[?] from the zero-bias transmission function evaluated at the Fermi level (E_F) of the leads,

$$\mathscr{G} = \mathscr{G}_0 T(E_F, V=0), \quad (4)$$

where $\mathscr{G}_0$ is the quantum unit of conductance ($2e^2/h$).

The matrix Green's function of the extended molecule is obtained from electronic structure calculations, usually based on mean-field DFT models, where the Hamiltonian matrix $\mathbf{H}_{EM}$ is approximated by the self-consistent Kohn–Sham Fock matrix (Fockian) $\mathbf{F}_{EM}$. Note that the electronic structure calculation on the EM does not include the effect of the leads, which is taken into account only via the self-energies in the

transmission calculation. In a fully self-consistent transport calculation, the DFT calculation is adjusted so that the electronic structure of the system is recalculated iteratively from the Green's function until convergence is achieved. In this scenario, periodic boundary conditions (PBC) are required not only for the leads but also for the extended molecule. However, a good approximation is realized by using a non-self-consistent Green's function built from the electronic structure of the EM calculated without PBC, combined with lead self-energies obtained from calculation where PBC is applied solely in the transport direction.[?] The disadvantage of this approach is that the band-like structure of the bulk spectra is not fully recovered, resulting in dense drops in the transmission function in the respective domains. These regions generally do not impact the interpretation of the transport in the vicinity of the Fermi level significantly. Despite these artifacts, such calculations are notably useful for simulating mechanically controlled break junction experiments where needle-like contacts are used. Additionally, employing finite EM calculations allows for a wider variety of electronic structure methods and computational tools to be utilized.

B. Huzinaga embedding approach

The combination of different DFT functionals for the molecule and the electrode domains of the EM can be achieved using an appropriate embedding technique. In this work we suggest the approach described by Hégely et al,[?] which is a formally exact, projection-based embedding method founded on the Huzinaga equation. The system (in our case, the extended molecule, *EM*) is divided into two predefined parts, shown in Figure **??**, the active subsystem (the molecule in the SMJ, denoted by *M*) and the environment (the metal clusters that model the electrodes, denoted by *El*). In the first step, a DFT calculation on the entire system (also called *supersystem* hereafter) is performed using the functional chosen for the environment, called functional I hereafter, solving the equations for the usual Kohn–Sham Fockian

$$\mathbf{F}_{EM} \;=\; \mathbf{h}+\mathbf{L}^{\mathrm{I}}[\mathbf{D}_{EM}] \tag{5}$$

where $\mathbf{h}$ is the core Hamiltonian of the supersystem and $\mathbf{L}^{\mathrm{I}}[\mathbf{D}_{EM}]$ stands for the two-electron and exchange-correlation part of the Kohn–Sham matrix, evaluated from the supersystem density $\mathbf{D}_{EM}$ using functional I. The matrix (formulated in the atomic orbital (AO) basis) can be divided into blocks corresponding to the subsystems as

$$\mathbf{F}_{EM} = \begin{pmatrix} \mathbf{F}_M & \mathbf{F}_{El-M} \\ (\mathbf{F}_{El-M})^{\mathrm{T}} & \mathbf{F}_{El} \end{pmatrix}. \tag{6}$$

The occupied molecular orbitals (MOs) produced in the first SCF step are then localized to the individual subsystems using the SPADE (Subsystem Projected AO DEcomposition) algorithm by Claudino and Mayhall.[?] The localized orbitals belonging to different fragments are used to construct the Fock matrix of the active subsystem under the influence of the *embedding potential*, obtained from density of the environment as

$$\tilde{\mathbf{F}} \;=\; \mathbf{h}+\mathbf{L}^{\mathrm{II}}[\tilde{\mathbf{D}}_M]+(\mathbf{L}^{\mathrm{I}}[\mathbf{D}_{EM}]-\mathbf{L}^{\mathrm{I}}[\mathbf{D}_M]), \tag{7}$$

with $\mathbf{L}^{\mathrm{II}}[\tilde{\mathbf{D}}_M]$ being the two-electron part of the Fockian of the molecule, evaluated using the functional chosen for the active domain, called functional II. The remaining terms in Eqn. **??** give the embedding potential. $\mathbf{D}_M$ denotes the density of the active subsystem obtained with functional I, while $\tilde{\mathbf{D}}_M$ is that of the embedded active subsystem, evaluated using functional II. The localized orbitals defining this latter density ($\tilde{\mathbf{C}}$) are obtained by solving the eigenvalue equations of the Fockian, with a constraint that the orthogonality of the orbitals of the different domains is enforced.[? ? ?] This is achieved by solving the Huzinaga-type equation[?]

$$(\tilde{\mathbf{F}}-\mathbf{S}\mathbf{P}^{\mathrm{o}}_{El}\tilde{\mathbf{F}}-\tilde{\mathbf{F}}\mathbf{P}^{\mathrm{o}}_{El}\mathbf{S}-\mathbf{S}\mathbf{P}^{\mathrm{v}}_{El}\tilde{\mathbf{F}}-\tilde{\mathbf{F}}\mathbf{P}^{\mathrm{v}}_{El}\mathbf{S}+2\mathbf{S}\mathbf{P}^{\mathrm{v}}_{El}\tilde{\mathbf{F}}\mathbf{P}^{\mathrm{v}}_{El}\mathbf{S})\tilde{\mathbf{C}} \;=\; \mathbf{S}\tilde{\mathbf{C}}\tilde{\boldsymbol{\varepsilon}}, \tag{8}$$

where $\mathbf{S}$ is the overlap matrix of the atomic orbitals, $\mathbf{P}^{\mathrm{o}}_{El}$ and $\mathbf{P}^{\mathrm{v}}_{El}$ are the projectors of the occupied and virtual orbitals of the environment, respectively, and $\tilde{\boldsymbol{\varepsilon}}$ is a diagonal matrix containing the orbital energies of the embedded orbitals. Further details of this embedding approach can be found in Refs. **? ? ? ?** .

The equations are solved in an iterative, self-consistent manner, producing the converged density $\tilde{\mathbf{D}}_M$ of the molecule. The supersystem Fockian is then constructed using the block of the Fock matrix obtained with functional II that corresponds to the AOs of the active subsystem ($\tilde{\mathbf{F}}_M$), with the remaining blocks taken from $\mathbf{F}_{EM}$ as

$$\tilde{\mathbf{F}}_{EM} := \begin{pmatrix} \tilde{\mathbf{F}}_M & \mathbf{F}_{El-M} \\ (\mathbf{F}_{El-M})^{\mathrm{T}} & \mathbf{F}_{El} \end{pmatrix}. \tag{9}$$

The eigenvectors of this supersystem Fockian provide the supersystem MOs, $\tilde{\mathbf{C}}_{EM}$. Note that during the second SCF procedure the embedding potential introduced in Eqn. **??** is kept constant, and only affects the $\tilde{\mathbf{F}}_M$ block.

The role of the orbitals of the molecule can be characterized by the overlap between the supersystem MOs and the orbitals localized to the molecule in the embedding calculation, given by

$$\bar{\mathbf{S}}^{max}_p := \max\left(\tilde{\mathbf{C}}^{\mathrm{T}}_{EM}\mathbf{S}\tilde{\mathbf{C}}\right)_{pq}, q \in M \tag{10}$$

where $\tilde{\mathbf{C}}$ contains the localized orbitals and the p and q denote the supersystem MOs and the orbitals localized to the molecule, respectively. This maximum element characterizes the extent to which the orbitals of the molecule can mix into a particular orbital of the EM.

As discussed in detail in Refs. **?** and **?** , the result of the embedding calculation depends on the choice of the virtual space in the second SCF procedure. In embedded correlation calculations (e.g. Wave function-in-DFT models) one normally aims at a virtual space that resembles that of an isolated active fragment to the highest possible extent, which is effectively achieved using a projected atomic orbital (PAO) procedure.[?] In the present DFT-in-DFT model this issue is of modest importance, as the embedded subsystem density is much less sensitive to the particular choice of this space. This

means that not just an appropriately parametrized PAO generation should provide satisfactory results, but applying the SPADE localization to the virtual domain, or even the adoption of the complete (untruncated) supersystem virtual space are viable options (see also Section **??** below).

C. Computational Details

The equilibrium structures of the isolated molecules were obtained from gas-phase optimization using the PBE functional and the aug-cc-pVDZ basis set. The Hartree–Fock and DFT calculations on these systems were carried out with the Turbomole[? ?] program system, while for the reference CCSD and CCSD(T)(a)* calculations (see below) the CFOUR program[?] was used. The core electrons were excluded from the correlation treatment in these calculations.

The EM model systems were built by placing the molecules between two gold clusters, representing the electrodes, in a configuration denoted as (III',III') in the classification by Quek et al.[?] Each electrode consisted of a 4-atomic tetrahedral gold tip unit attached to six 3x3 Au(111) atomic layers, corresponding to two principal layers, with an Au-Au distance of 2.885 Å. The stacking of the layers was done to comply with one-dimensional periodic calculations,[?] simulating the needle-like contacts of break-junction experiments. The constructed EM models were subsequently optimized using the PBE functional, under the constraint that only the molecule and the gold tip units were allowed to undergo structural changes. The structure of the BDA extended molecule obtained from this procedure is shown in Figure **??**, while coordinates for all EM models are available in the *Supplementary material*. For comparisons with results from Ref. **?** , another EM model with BDA was built using the structure of the molecule and gap parameters taken from that work, that is, the distance between the Au atom tips set to 9.90 Å and the N-Au distances tuned to 2.55 Å. This system is given in Table S8. Gold clusters identical to those in the EM models, without the tetrahedral tip unit, were used as the supercell in the periodic lead calculations.

In the optimization of the EM models and the DFT-in-DFT embedding calculations, the aug-cc-pVDZ basis set was used on the atoms of the molecules, while for the gold atoms the cc-pVDZ-PP basis set,[?] in combination with the def-PP-ECP effective core potential (ECP),[?] was applied. The embedding calculations were done with the MRCC program system.[? ?] As the fitting basis in the SCF calculations, the universal basis by Weigend[?] was used.

The calculations for the leads were carried out with the Turbomole RIPER program[?] using the PBE functional, with the basis set, effective core potentials and fitting basis matching those in the embedding calculations. The periodic boundary conditions were applied only in the transport direction, resulting in a Fermi level of 5.20 eV, which is in good agreement with the experimental value of 5.31 eV.[?]

The zero-bias transmission functions (Eqns. **??** and **??**) were calculated using an in-house Python code. In this implementation the non-self-consistent matrix Green's function is constructed from the Fock matrix of the EM, obtained either through supersystem DFT (see Eqn. **??**) or DFT-in-DFT embedding (see Eqn. **??**) calculations, with the η parameter set to $3 \cdot 10^{-3}$ eV. The self-energies are computed from the results of the periodic calculations for the lead, based on the standard decimation technique[?] as described in detail in Appendix D of Ref. **?** . The transmission functions are evaluated from -7.0 eV to 0.0 eV on a uniform grid with 0.01 eV resolution.

III. RESULTS AND DISCUSSION

A. Benchmarking functionals on the isolated molecules

A principle requirement for a DFT functional suitable for transport calculations is to accurately predict the IPs and EAs by the orbital energies of the molecule in gas phase. Therefore, various functionals were benchmarked against a high-level many-body correlated method for the isolated molecules. Besides the Hartree-Fock (HF) method, the PBE functional and the PBE0[?] and B3LYP[?] hybrid functionals have been evaluated. Furthermore, the HSE06[?] and CAM-B3LYP[?] range-separated hybrids were also considered, as this type of functionals were previously identified as favourable choices for IP and EA predictions.[? ?] As reference, the EOM-CCSD(T)(a)* model by Matthews and Stanton[?] was used for BDA, which has been found previously a very accurate pseudotriples coupled-cluster variant for similar applications.[? ? ?] For Me_4-BDA and F_4-BDA, EOM-CCSD reference data were acquired. Figure **??** shows the first three IPs and EAs of the investigated molecules, as predicted by the various methods using different basis sets. The individual values are available in the *Supplementary material*.

By comparing to the reference, it is clear that the PBE functional shows the largest errors, about 3 eV for all IPs, regardless of the basis set. For the EAs, the errors of PBE are generally smaller, between 1.2 eV and 2.2 eV in absolute terms if diffuse basis sets are used (which should normally be the choice for calculating anionic systems). However, the wrong sign of the EA in all such cases is particularly alarming that the energy levels predicted by this functional are qualitatively wrong for the investigated molecules.

The tested hybrid functionals, as well as the HSE06 range-separated hybrid all show a significant, 1.6 eV – 2.6 eV underestimation for the IPs, which is also surprisingly insensitive to the basis set size. The error increases with the order of ionization, indicating that simply shifting the spectra by a chosen constant should not be expected to mitigate the inaccuracy of these methods in a general way. The absolute errors of the electron affinities in diffuse basis sets are below 1 eV in most cases, except for F_4-BDA where the values are notably larger, up to 1.8 eV. Moreover, almost all predicted values still have the wrong sign. The only functional providing satisfactory results in this regard is CAM-B3LYP which also shows the smallest deviation from the reference in absolute terms. Furthermore, this functional also shows the best accuracy for the IPs among the tested variants, with an underestimation below 0.7 eV, which shows a remarkably small variation with the

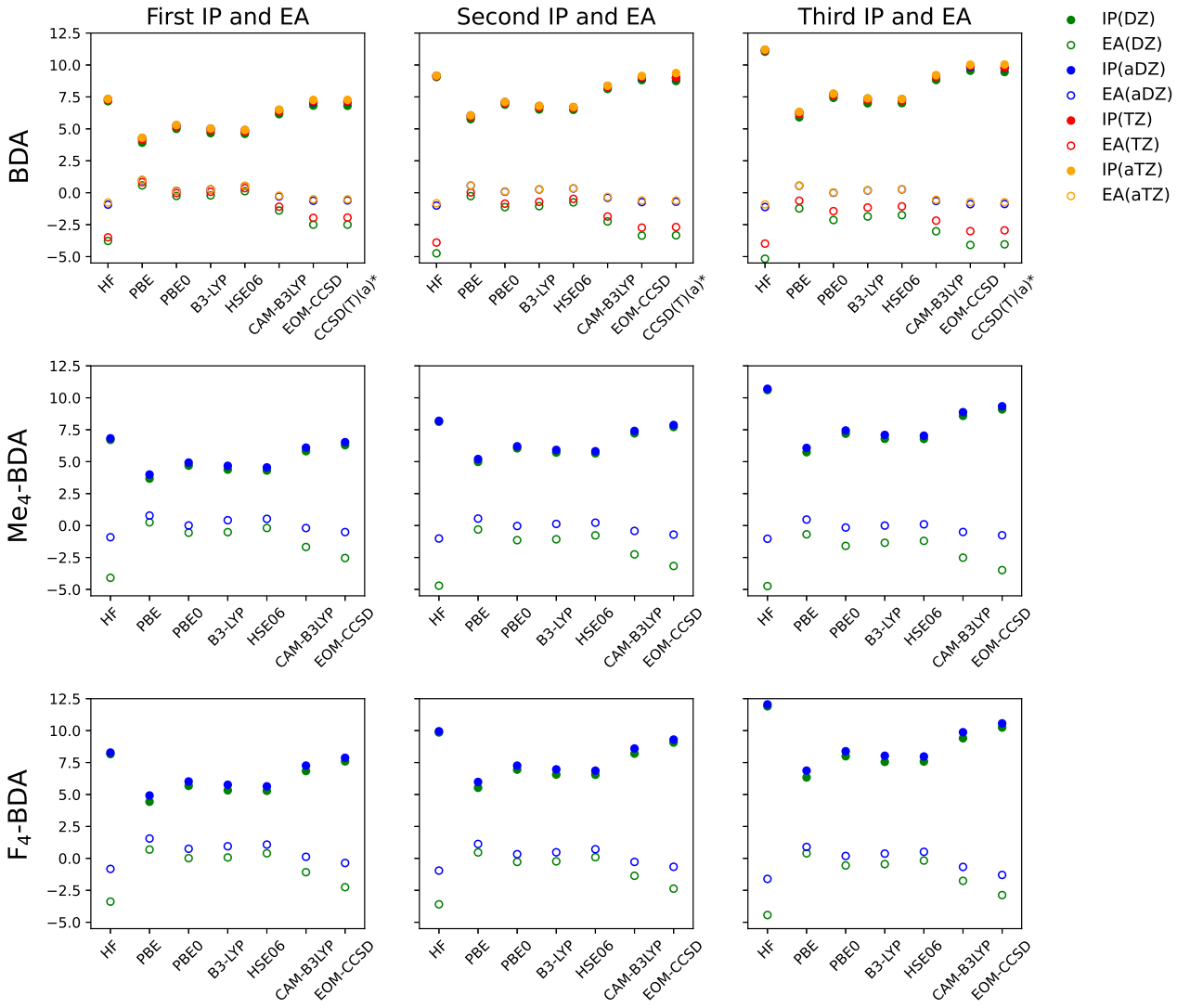

FIG. 2. The first three ionization potentials (IPs) and electron affinities (EAs) of the isolated BDA, Me_4-BDA and F_4-BDA molecules in electron volts, using the cc-pVDZ (DZ), cc-pVTZ (TZ), aug-cc-pVDZ (aDZ), and aug-cc-pVTZ (aTZ) basis sets. In HF and DFT calculations the IP and EA values are obtained as the opposites of the corresponding orbital energies, according to Koopmans' theorem.

basis set or the state in question. The difference is particularly notable for F_4-BDA where no other functional produced an error below 2 eV for any IP. This benchmark indicates that CAM-B3LYP clearly stands out as the best DFT functional for the BDA analogues, providing reasonable energy levels even without empirical shifts or corrections.

B. Transport calculations on the SMJs

Transport calculations according to Section **??** have been performed for SMJs containing the BDA, Me_4-BDA and F_4-BDA molecules, using the embedding schema introduced in Section **??** in a CAM-B3LYP-in-PBE fashion for the extended molecule, that is, the CAM-B3LYP functional was used for the molecule and PBE for the electrodes. For both the occupied and the virtual domains of the active subsystem the SPADE localization was used (see the end of Section **??** for details). To investigate the effect of the localization scheme, the BDA transport curves calculated with different virtual spaces are also shown in the *Supplementary material*. The results are remarkably insensitive to the particular choice of this space, with the transmission curves showing minuscule variations in the vicinity of E_F depending on the virtual space used. For comparison, calculations using PBE across the entire EM systems were also performed.

Figure **??** shows the transmission curves (see Eqn. **??**) of the BDA SMJ on a logarithmic scale, obtained from the supersystem PBE and the embedding calculations. The results obtained for Me_4-BDA and F_4-BDA are shown on Figures S2 and S3, respectively. The CAM-B3LYP-in-PBE curve in Figure **??** runs below PBE in almost the entire investigated energy

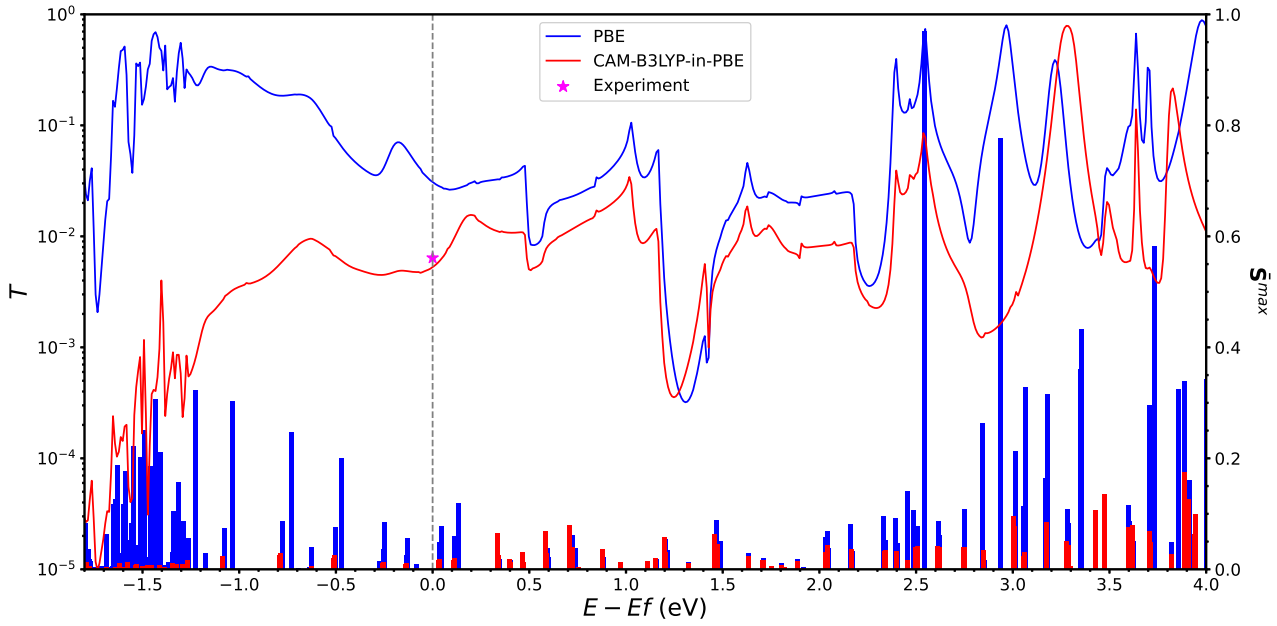

FIG. 3. Transmission function (T) obtained from the supersystem PBE (blue curve) and CAM-B3LYP-in-PBE embedding (red curve) calculations for the BDA SMJ. The Fermi level is marked with gray dashed line , while the magenta asterisk indicates the experimental conductance[?] value. The maximum overlaps ($\bar{\mathbf{S}}^{max}$) of the EM eigenvectors with localized orbitals of the embedded molecule (see Eqn. **??**) at the PBE level are shown with blue bars, while those from the CAM-B3LYP-in-PBE model are shown in red.

range and a similar behavior is observed for F_4-BDA. In the case of the Me_4-BDA system the CAM-B3LYP-in-PBE curve follows this trend up to 0.5 eV above the Fermi level, indicating that the embedding model predicts significantly lower transmissions around E_F than ordinary PBE. This can be regarded as an improvement, as PBE was previously found to overestimate the experimental conductivity of all investigated variants.[? ?]

In Table **??**, the zero-bias (E_F) conductance values are shown numerically. The value obtained for BDA with supersystem PBE is in line with that of Jin et al.,[?] considering also the significant differences in the calculation methodology and the SMJ model structures. With the CAM-B3LYP-in-PBE embedding, a reduction of the PBE transmission by a factor of 5.8 is observed, the predicted value showing much better agreement with the experimental value. The absolute error ($1.1 \cdot 10^{-3}\mathscr{G}_0$) is now comparable to that of the computationally much more expensive GW transport technique ($2.8 \cdot 10^{-3}\mathscr{G}_0$) published by Jin and co-workers.[?] A similar decrease of the CAM-B3LYP-in-PBE conductance with respect to the PBE one can be seen for F_4-BDA, that is, by a factor of 5.9, nevertheless the absolute error relative to the experimental value is somewhat larger ($2.7 \cdot 10^{-3}\mathscr{G}_0$). For Me_4-BDA the PBE value is reduced by a factor of 3.3 with CAM-B3LYP-in-PBE, the calculated transmission still considerably overestimating the experiment (by a factor of 1.9). This in contrast to the case of BDA and F_4-BDA, where a slight underestimation of the experimental conductance is found. The agreement is, nevertheless, significantly improved compared to PBE and the embedding model correctly reproduces also the trend of the measured conductivity in the F_4-BDA, BDA, Me_4-BDA series. Nevertheless, the relative differences between the different variants appear to be exaggerated by the embedding calculations. The reason behind this finding may be the fact that the predicted values are nominally much smaller, which magnifies the impact of other possible sources of inaccuracy, in particular the sensitivity of the simulation to the structural parameters of the SMJ. This is illustrated on Fig. S4 where the transmission functions for the BDA system are presented also with the geometry sourced from Ref. **?** , showing a notable difference of the predicted values around E_F. A comparison to the respective supersystem PBE results indicates that the embedding model is clearly more sensitive to the structure.

Figure **??** also shows the maximum overlaps $\bar{\mathbf{S}}_p^{max}$ (see Eqn. **??**) of the supersystem MOs with those localized to the BDA molecule in the embedding method, evaluated at the corresponding EM orbital energies. The identical quantities for the ordinary PBE calculations, shown as blue bars in Fig.**??**, are those obtained from a PBE-in-PBE embedding model. Note that in this latter variant the embedding is exact, that is, it produces the same density for the EM as that of a supersystem PBE calculation and the embedding is used solely to distribute the density into the subsystems using the same orbital localization methodology. Generally, maxima in the transmission curve are accompanied by increased maximum overlaps at the adjacent EM eigenvalues, indicating that the charge transmission is larger where some molecular states can mix more strongly with those of the electrodes in the EM orbitals. Since most EM orbitals with energies around E_F are predominantly those of the electrode domains,[?] this finding is in line with the

TABLE I. Calculated and experimental zero-bias conductances ($\mathscr{G}$) in units of $10^{-3}\mathscr{G}_0$ ($= 2\cdot 10^{-3}\, e^2/h$)

Method	$\mathscr{G}$(Me$_4$-BDA)	$\mathscr{G}$(BDA)	$\mathscr{G}$(F$_4$-BDA)
Experimental[a]	8.2±0.2	6.4±0.2	5.5±0.2
GW[b]	4.15	3.67	1.74
PBE	52.2	30.9	16.7
CAM-B3LYP-in-PBE	15.8	5.3	2.8

[a] Experimental values taken from Ref. **?** .
[b] Values taken from Ref. **?** .

interpretation of the transport as the result of a perturbation of the electrode states by the molecule. By comparing the PBE and the embedding results in Figure **??**, a drop in the $\bar{\mathbf{S}}_p^{max}$ values in the latter case is clearly observable. This phenomenon should be a consequence of the change of the energy levels of BDA in the CAM-B3LYP model, shifting the orbitals of the molecule away from those of the electrodes in the investigated energy domain.

This is also demonstrated in Table **??** which shows for all systems the energies associated with the three highest occupied and three lowest unoccupied localized orbitals of the molecules, i. e. the eigenvalues ($\tilde{\boldsymbol{\varepsilon}}$) of the Huzinaga operator that correspond to the active subsystem. The numbers show that by employing the CAM-B3LYP functional to the molecule, the orbital energies are shifted to lower values for the occupied orbitals and to higher values for virtual orbitals, respectively. The Fermi level of the electrodes falls into the HOMO-LUMO gap which increases almost two-fold (7.98 eV, 7.84 eV, and 8.56 eV with the embedding model vs. 4.06 eV, 4.33 eV, and 4.48 eV with PBE for the BDA, Me$_4$-BDA, and F$_4$-BDA systems, respectively). A larger discrepancy of the molecular and electrode energy levels reduces the extent of mixing between the corresponding eigenvectors, resulting in a lower predicted transmission at the affected energies.

This finding is in line with the philosophy of the DFT+Σ techniques[? ? ?] that manually shift the eigenvalue spectrum of the molecular block by a chosen constant. However, the introduction of such tuning parameters into the model reduces the generality and robustness of these methods and the use of a constant shift for all orbitals should not be appropriate at cases where several molecular levels affect the transmission around E_F. The proposed embedding model is free of such ambiguities.

IV. CONCLUSION

Single-molecule junctions are challenging systems for electronic structure modeling due to the qualitatively different properties of the metal and molecule domains. In this study we presented an alternative methodology for transport calculations in SMJs that allows a selection of the exchange-correlation functionals such that each part of the system is described with an appropriate method. This is achieved by a formally exact projection-based DFT-in-DFT embedding approach which does not deteriorate the computational scaling of the method. In fact, since the molecule represents a relatively small part of the SMJ, the embedding calculation involves a minimal computational overhead compared to a simple supersystem calculation, even if a sophisticated exchange-correlation functional is used for the active subsystem.

The performance of the proposed methodology was demonstrated by transport calculations on SMJs involving BDA, Me$_4$-BDA, and F$_4$-BDA. By using a DFT functional for the molecules that is found to be appropriate on the basis of simple gas phase property calculations, the accuracy of the predicted zero-bias conductance could be improved significantly compared to a conventional modeling that uses the PBE functional for the whole system. The performance is found to approach that of the computationally much more expensive many-body models. The reason of the observed enhancement could be explained by analyzing changes in the molecular energy levels and the entanglement of the molecule and electrode wave functions.

Nevertheless, we do not regard the presented application as the overall limit of the accuracy that is achievable with the embedding approach. The use of a better suited DFT functional for the different domains, that of a more complete basis set, or the adoption of a high-level wave function-based model for the active subsystem could potentially deliver even superior performance. We consider the principal advantage of the embedding approach that it allows to design an appropriate methodology without the need of tuning parameters for the transport calculations, e.g. by introducing artificial spectrum shifts.

ACKNOWLEDGMENTS

This work was founded by the National Research, Development and Innovation Fund (NKFIF) of Hungary, Grant No. 142634. D.P.J. acknowledges support by the ÚNKP-23-3 New National Excellence Program of the Ministry for Culture and Innovation from the source of the National Research, Development and Innovation Fund. The authors thank Prof. Jos M. Thijssen, Dr. Bence Hégely and Prof. Mihály Kállay for useful discussions. The authors are grateful for the computational resources of the DelftBlue supercomputer,[?] provided by Delft High Performance Computing Centre (https://www.tudelft.nl/dhpc).

SUPPLEMENTARY MATERIAL

The *Supplementary material* supplied with this article presents the coordinates of the investigated molecules (Tables S2-S4), the SMJs (Tables S5-S8) and lead model systems (Table S1 and Figure S1). The first three IP and EA values of the gas-phase molecules, calculated at different levels with different basis sets are summarized in Tables S9-S11. The calculated transmission functions of Me$_4$-BDA and F$_4$-BDA are illustrated on Figures S2 and S3, respectively. The comparison of BDA transmission functions obtained in different

TABLE II. Orbital energies ($\tilde{\epsilon}$, in eV) of the three highest occupied (HOMO-2, HOMO-1, HOMO) and lowest virtual (LUMO, LUMO+1, LUMO+2) molecular orbitals of the embedded subsystem, obtained from PBE-in-PBE and CAM-B3LYP-in-PBE embedding calculations on the extended molecule. Values relative to the Fermi level ($E_F = 5.20$) are shown in parentheses.

	HOMO-2		HOMO-1		HOMO		LUMO		LUMO+1		LUMO+2	
						BDA						
PBE-in-PBE	−8.55	(−3.35)	−6.75	(−1.55)	−6.48	(−1.28)	−2.10	(3.10)	−1.76	(3.44)	−1.02	(4.18)
CAM-B3LYP-in-PBE	−11.25	(−6.05)	−8.91	(−3.71)	−8.42	(−3.22)	−0.16	(5.04)	0.07	(5.27)	0.09	(5.29)
						Me_4-BDA						
PBE-in-PBE	−8.92	(−3.72)	−7.62	(−2.42)	−6.78	(−1.58)	−2.62	(2.58)	−2.15	(3.05)	−1.21	(3.99)
CAM-B3LYP-in-PBE	−11.66	(−6.46)	−9.87	(−4.67)	−8.78	(−3.58)	−0.69	(4.51)	−0.38	(4.82)	−0.01	(5.19)
						F_4-BDA						
PBE-in-PBE	−8.67	(−3.47)	−7.14	(−1.94)	−6.81	(−1.61)	−2.33	(2.87)	−2.20	(3.00)	−2.16	(3.04)
CAM-B3LYP-in-PBE	−11.63	(−6.43)	−9.71	(−4.51)	−9.03	(−3.83)	−0.47	(4.73)	−0.41	(4.79)	−0.36	(4.84)

geometries and from different virtual space localizations are shown on Figures S4 and S5, respectively.

DATA AVAILABILITY STATEMENT

The data that support the findings of this study are available in the article (and its *Supplementary material*).

CONFLICT OF INTEREST STATEMENT

The author authors have no conflicts to disclose.

P. Gehring, J. M. Thijssen, and H. S. van der Zant, "Single-molecule quantum-transport phenomena in break junctions," Nature Reviews Physics **1**, 381–396 (2019).

P. T. Mathew and F. Fang, "Advances in molecular electronics: A brief review," Engineering **4**, 760–771 (2018).

M. Thoss and F. Evers, "Perspective: Theory of quantum transport in molecular junctions," The Journal of Chemical Physics **148**, 030901 (2018), https://pubs.aip.org/aip/jcp/article-pdf/doi/10.1063/1.5003306/19971546/030901_1_1.5003306.pdf.

M. Brandbyge, J.-L. Mozos, P. Ordejón, J. Taylor, and K. Stokbro, "Density-functional method for nonequilibrium electron transport," Phys. Rev. B **65**, 165401 (2002).

Y. Xue, S. Datta, and M. A. Ratner, "First-principles based matrix green's function approach to molecular electronic devices: general formalism," Chem. Phys. **281**, 151–170 (2002).

J. P. Perdew, K. Burke, and M. Ernzerhof, "Generalized gradient approximation made simple," Phys. Rev. Lett. **77**, 3865–3868 (1996).

S. Y. Quek, L. Venkataraman, H. J. Choi, S. G. Louie, M. S. Hybertsen, and J. B. Neaton, "Amine-gold linked single-molecule circuits: Experiment and theory," Nano Lett. **11**, 3477 (2007).

J. A. Celis Gil and J. M. Thijssen, "Transport gap renormalization at a metal-molecule interface using DFT-NEGF and spin unrestricted calculations," The Journal of Chemical Physics **147**, 084102 (2017), https://pubs.aip.org/aip/jcp/article-pdf/doi/10.1063/1.4999469/15531319/084102_1_online.pdf.

S. Y. Quek, H. J. Choi, S. G. Louie, and J. B. Neaton, "Length dependence of conductance in aromatic single-molecule junctions," Nano Letters **9**, 3949–3953 (2009), pMID: 19751067, https://doi.org/10.1021/nl9021336.

T. Markussen, C. Jin, and K. S. Thygesen, "Quantitatively accurate calculations of conductance and thermopower of molecular junctions," physica status solidi (b) **250**, 2394–2402 (2013), https://onlinelibrary.wiley.com/doi/pdf/10.1002/pssb.201349217.

L. Reining, "The gw approximation: content, successes and limitations," WIREs Computational Molecular Science **8**, e1344 (2018), https://wires.onlinelibrary.wiley.com/doi/pdf/10.1002/wcms.1344.

K. S. Thygesen and A. Rubio, "Conserving *gw* scheme for nonequilibrium quantum transport in molecular contacts," Phys. Rev. B **77**, 115333 (2008).

C. Rostgaard, K. W. Jacobsen, and K. S. Thygesen, "Fully self-consistent gw calculations for molecules," Phys. Rev. B **81**, 085103 (2010).

X. Blase, C. Attaccalite, and V. Olevano, "First-principles *GW* calculations for fullerenes, porphyrins, phtalocyanine, and other molecules of interest for organic photovoltaic applications," Phys. Rev. B **83**, 115103 (2011).

B. Holm and U. von Barth, "Fully self-consistent GW self-energy of the electron gas," Phys. Rev. B **57**, 2108–2117 (1998).

J. M. Garcia-Lastra, C. Rostgaard, A. Rubio, and K. S. Thygesen, "Polarization-induced renormalization of molecular levels at metallic and semiconducting surfaces," Phys. Rev. B **80**, 245427 (2009).

J. B. Neaton, M. S. Hybertsen, and S. G. Louie, "Renormalization of molecular electronic levels at metal-molecule interfaces," Phys. Rev. Lett. **97**, 216405 (2006).

M. Strange, C. Rostgaard, H. Häkkinen, and K. S. Thygesen, "Self-consistent gw calculations of electronic transport in thiol- and amine-linked molecular junctions," Phys. Rev. B **83**, 115108 (2011).

C. Jin, M. Strange, T. Markussen, G. C. Solomon, and K. S. Thygesen, "Energy level alignment and quantum conductance of functionalized metal-molecule junctions: Density functional theory versus GW calculations," The Journal of Chemical Physics **139**, 184307 (2013), https://pubs.aip.org/aip/jcp/article-pdf/doi/10.1063/1.4829520/9528378/184307_1_online.pdf.

D. A. Egger, S. Weissman, S. Refaely-Abramson, S. Sharifzadeh, M. Dauth, R. Baer, S. Kümmel, J. B. Neaton, E. Zojer, and L. Kronik, "Outer-valence electron spectra of prototypical aromatic heterocycles from an optimally tuned range-separated hybrid functional," Journal of Chemical Theory and Computation **10**, 1934–1952 (2014), pMID: 24839410, https://doi.org/10.1021/ct400956h.

S. Fürst and M. Kaupp, "Accurate ionization potentials, electron affinities, and band gaps from the ωlh22t range-separated local hybrid functional: No tuning required," Journal of Chemical Theory and Computation **19**, 3146–3158 (2023), pMID: 37204113, https://doi.org/10.1021/acs.jctc.3c00173.

W. Gao, T. A. Abtew, T. Cai, Y.-Y. Sun, S. Zhang, and P. Zhang, "On the applicability of hybrid functionals for predicting fundamental properties of metals," Solid State Communications **234-235**, 10–13 (2016).

J. Yang, S. Falletta, and A. Pasquarello, "Range-separated hybrid functionals for accurate prediction of band gaps of extended systems," npj Computational Materials **9**, 108 (2023).

A. Yamada, Q. Feng, A. Hoskins, K. D. Fenk, and B. D. Dunietz, "Achieving predictive description of molecular conductance by using a range-separated hybrid functional," Nano Letters **16**, 6092–6098 (2016), pMID: 27636328, https://doi.org/10.1021/acs.nanolett.6b02241.

Z.-F. Liu, D. A. Egger, S. Refaely-Abramson, L. Kronik, and J. B. Neaton, "Energy level alignment at molecule-metal interfaces from an optimally tuned range-separated hybrid functional," The Journal of Chemical Physics **146**, 092326 (2017), https://pubs.aip.org/aip/jcp/article-pdf/doi/10.1063/1.4975321/14049633/092326_1_online.pdf.

S. Bhandari, A. Yamada, A. Hoskins, J. Payne, H. Aksu, and B. D. Dunietz, "Achieving predictive description of negative differential resistance in molecular junctions using a range-separated hybrid functional," Advanced Theory and Simulations **4**, 2000016 (2021), https://onlinelibrary.wiley.com/doi/pdf/10.1002/adts.202000016.

L. Venkataraman, J. E. Klare, C. Nuckolls, M. S. Hybertsen, and M. L. Steigerwald, "Dependence of single-molecule junction conductance on molecular conformation," Nature **442**, 7105 (2006).

M. Dell'Angela, G. Kladnik, A. Cossaro, A. Verdini†, M. Kamenetska, I. Tamblyn, S. Y. Quek, J. B. Neaton, D. Cvetko, and A. V. L. Morgante, "Relating Energy Level Alignment and Amine-Linked Single Molecule Junction Conductance," Nano Lett. **10**, 2470 (2010).

J. Ning, R. Li, X. Shen, Z. Qian, S. Hou, A. R. Rocha, and S. Sanvito, "First-principles calculation on the zero-bias conductance of a gold/1,4-diaminobenzene/gold molecular junction," Nanotec. **18**, 345203 (2007).

M. S. Hybertsen, L. Venkataraman, J. E. Klare, A. C. Whalley, M. L. Steigerwald, and C. Nuckolls, "Amine-linked single-molecule circuits: systematic trends across molecular families," J. Phys. Cond. Mat. **20**, 374115 (2008).

L. Venkataraman, Y. S. Park, A. C. Whalley, C. Nuckolls, M. S. Hybertsen, and M. L. Steigerwald, "Electronics and chemistry: Varying single-molecule junction conductance using chemical substituents," Nano Letters **7**, 502–506 (2007), pMID: 17253760, https://doi.org/10.1021/nl062923j.

Y. Meir and N. S. Wingreen, "Landauer formula for the current through an interacting electron region," Phys. Rev. Lett. **68**, 2512 (1992).

M. P. L. Sancho, J. M. L. Sancho, J. M. L. Sancho, and J. Rubio, "Highly convergent schemes for the calculation of bulk and surface green functions," Journal of Physics F: Metal Physics **15**, 851 (1985).

C. J. O. Verzijl and J. M. Thijssen, "Dft-based molecular transport implementation in adf/band," The Journal of Physical Chemistry C **116**, 24393–24412 (2012), https://doi.org/10.1021/jp3044225.

J. C. Cuevas and E. Scheer, *Molecular Electronics* (World Scientific, Singapore, 2010) https://www.worldscientific.com/doi/pdf/10.1142/7434.

I. Baldea, *Molecular Electronics : An Experimental and Theoretical Approach* (Pan Stanford Publishing Pte Ltd, Singapore, 2015).

R. Landauer, "Conductance determined by transmission: probes and quantised constriction resistance," J. Condens. Matter Phys. **1**, 8099 (1989).

C. J. O. Verzijl, J. S. Seldenthuis, and J. M. Thijssen, "Applicability of the wide-band limit in DFT-based molecular transport calculations," The Journal of Chemical Physics **138**, 094102 (2013), https://pubs.aip.org/aip/jcp/article-pdf/doi/10.1063/1.4793259/13955390/094102_1_online.pdf.

B. Hégely, P. R. Nagy, G. G. Ferenczy, and M. Kállay, "Exact density functional and wave function embedding schemes based on orbital localization," J. Comp. Phys. **145**, 064107 (2016).

D. Claudino and N. J. Mayhall, "Automatic partition of orbital spaces based on singular value decomposition in the context of embedding theories," Journal of Chemical Theory and Computation **15**, 1053–1064 (2019).

F. R. Manby, M. Stella, J. D. Goodpaster, and T. F. I. Miller, "A simple, exact density-functional-theory embedding scheme," Journal of Chemical Theory and Computation **8**, 2564–2568 (2012), pMID: 22904692, https://doi.org/10.1021/ct300544e.

Y. G. Khait and M. R. Hoffmann, "Chapter three - on the orthogonality of orbitals in subsystem kohn–sham density functional theory," in *Annual Reports in Computational Chemistry*, Annual Reports in Computational Chemistry, Vol. 8, edited by R. A. Wheeler (Elsevier, 2012) pp. 53–70.

Á. B. Szirmai, B. Hégely, A. Tajti, M. Kállay, and P. G. Szalay, "Projected atomic orbitals as optimal virtual space for excited state projection-based embedding calculations," Journal of Chemical Theory and Computation **20**, 3420–3425 (2024), pMID: 38626416, https://doi.org/10.1021/acs.jctc.4c00104.

A. T. Ádám B. Szirmai, Bónis Barcza and P. G. Szalay, "Accuracy of projected atomic virtual orbital space in embedding applications," Molecular Physics **122**, e2355694 (2024), https://doi.org/10.1080/00268976.2024.2355694.

J. Csóka, B. Hégely, P. R. Nagy, and M. Kállay, "Development of analytic gradients for the Huzinaga quantum embedding method and its applications to large-scale hybrid and double hybrid DFT forces," The Journal of Chemical Physics **160**, 124113 (2024), https://pubs.aip.org/aip/jcp/article-pdf/doi/10.1063/5.0194463/19847321/124113_1_5.0194463.pdf.

"TURBOMOLE V7.7 2022, a development of University of Karlsruhe and Forschungszentrum Karlsruhe GmbH, 1989-2007, TURBOMOLE GmbH, since 2007; available from `https://www.turbomole.org`.".

S. G. Balasubramani, G. P. Chen, S. Coriani, M. Diedenhofen, M. S. Frank, Y. J. Franzke, F. Furche, R. Grotjahn, M. E. Harding, C. Hättig, A. Hellweg, B. Helmich-Paris, C. Holzer, U. Huniar, M. Kaupp, A. Marefat Khah, S. Karbalaei Khani, T. Müller, F. Mack, B. D. Nguyen, S. M. Parker, E. Perlt, D. Rappoport, K. Reiter, S. Roy, M. Rückert, G. Schmitz, M. Sierka, E. Tapavicza, D. P. Tew, C. van Wüllen, V. K. Voora, F. Weigend, A. Wodyński, and J. M. Yu, "Turbomole: Modular program suite for ab initio quantum-chemical and condensed-matter simulations," J. Chem. Phys. **152**, 184107 (2020), https://doi.org/10.1063/5.0004635.

D. A. Matthews, L. Cheng, M. E. Harding, F. Lipparini, S. Stopkowicz, T.-C. Jagau, P. G. Szalay, J. Gauss, and J. F. Stanton, "Coupled-cluster techniques for computational chemistry: The cfour program package," The Journal of Chemical Physics **152**, 214108 (2020).

M. Strange, C. Rostgaard, H. Häkkinen, and K. S. Thygesen, "Self-consistent gw calculations of electronic transport in thiol- and amine-linked molecular junctions," Phys. Rev. B **83**, 115108 (2011).

K. A. Peterson and C. Puzzarini, "Systematically convergent basis sets for transition metals. ii. pseudopotential-based correlation consistent basis sets for the group 11 (cu, ag, au) and 12 (zn, cd, hg) elements," Theor. Chem. Acc. **114**, 283–296 (2005).

D. Figgen, G. Rauhut, M. Dolg, and H. Stoll, "Energy-consistent pseudopotentials for group 11 and 12 atoms: adjustment to multi-configuration dirac–hartree–fock data," Chem. Phys. **311**, 227–244 (2005).

M. Kállay, P. R. Nagy, D. Mester, Z. Rolik, G. Samu, J. Csontos, J. Csóka, P. B. Szabó, L. Gyevi-Nagy, B. Hégely, I. Ladjánszki, L. Szegedy, B. Ladóczki, K. Petrov, M. Farkas, P. D. Mezei, and A. Ganyecz, "The mrcc program system: Accurate quantum chemistry from water to proteins," The Journal of Chemical Physics **152**, 074107 (2020).

"Mrcc, a quantum chemical program suite written by m. kállay, p. r. nagy, z. rolik, d. mester, g. samu, j. csontos, j. csóka, b. p. szabó, l. gyevi-nagy, i. ladjánszki, l. szegedy, b. ladóczki, k. petrov, m. farkas, p. d. mezei, and b. hégely. see also z. rolik, l. szegedy, i. ladjánszki, b. ladóczki, and m. kállay, j. chem. phys. 139, 094105 (2013), as well as: `www.mrcc.hu`.".

F. Weigend, "Accurate coulomb-fitting basis sets for h to rn," Phys. Chem. Chem. Phys. **8**, 1057–1065 (2006).

H. B. Michaelson, "The work function of the elements and its periodicity," Journal of Applied Physics **48**, 4729–4733 (1977), https://pubs.aip.org/aip/jap/article-pdf/48/11/4729/18378039/4729_1_online.pdf.

F. Guinea, C. Tejedor, F. Flores, and E. Louis, "Effective two-dimensional hamiltonian at surfaces," Phys. Rev. B **28**, 4397–4402 (1983).

C. Adamo and V. Barone, "Toward reliable density functional methods without adjustable parameters: The PBE0 model," The Journal of Chemical Physics **110**, 6158–6170 (1999), https://pubs.aip.org/aip/jcp/article-pdf/110/13/6158/19068890/6158_1_online.pdf.

A. D. Becke, "Density-functional thermochemistry. III. The role of exact exchange," The Journal of Chemical Physics **98**, 5648–5652 (1993), https://pubs.aip.org/aip/jcp/article-pdf/98/7/5648/19277469/5648_1_online.pdf.

A. V. Krukau, O. A. Vydrov, A. F. Izmaylov, and G. E. Scuseria, "Influence of the exchange screening parameter on the performance of screened hybrid functionals," The Journal of Chemical Physics **125**, 224106 (2006), https://pubs.aip.org/aip/jcp/article-pdf/doi/10.1063/1.2404663/13263224/224106_1_online.pdf.

T. Yanai, D. P. Tew, and N. C. Handy, "A new hybrid exchange–correlation functional using the coulomb-attenuating method (cam-b3lyp)," Chemical Physics Letters **393**, 51–57 (2004).

D. A. Matthews and J. F. Stanton, "A new approach to approximate equation-of-motion coupled cluster with triple excitations," The Journal of Chemical Physics **145**, 124102 (2016), https://doi.org/10.1063/1.4962910.

A. Shaalan Alag, D. P. Jelenfi, A. Tajti, and P. G. Szalay, "Accurate prediction of vertical ionization potentials and electron affinities from spin-component scaled cc2 and adc(2) models," Journal of Chemical Theory and Computation **18**, 6794–6801 (2022), pMID: 36269873, https://doi.org/10.1021/acs.jctc.2c00624.

D. Kánnár, A. Tajti, and P. G. Szalay, "Accuracy of coupled cluster excitation energies in diffuse basis sets," Journal of Chemical Theory and Computation **13**, 202–209 (2017), pMID: 27959525, https://doi.org/10.1021/acs.jctc.6b00875.

A. Tajti, J. F. Stanton, D. A. Matthews, and P. G. Szalay, "Accuracy of coupled cluster excited state potential energy surfaces," Journal of Chemical Theory and Computation **14**, 5859–5869 (2018), pMID: 30299948, https://doi.org/10.1021/acs.jctc.8b00681.

D. P. Jelenfi, A. Tajti, and P. G. Szalay, "Interpretation of molecular electron transport in ab initio many-electron framework incorporating zero-point nuclear motion effects," Journal of Computational Chemistry **45**, 1968–1979 (2024), https://onlinelibrary.wiley.com/doi/pdf/10.1002/jcc.27381.

Delft High Performance Computing Centre (DHPC), "DelftBlue Supercomputer (Phase 2)," `https://www.tudelft.nl/dhpc/ark:/44463/DelftBluePhase2` (2024).